Check for updates

# Ratiometric two-photon fluorescent probe for *in situ* imaging of carboxylesterase (CE)-mediated mitochondrial acidification during medication†

Ao Jiang,[a] Guang Chen, [iD] *[a] Jie Xu,[a] Yuxia Liu, [iD] [a] Guanghui Zhao,[a] Zhenjun Liu,[a] Tao Chen,[ab] Yulin Li[ab] and Tony D. James [iD] *[ac]

We report on a dual ratiometric two-photon fluorescent probe for *in situ* sensing of mitochondrial CE activity and pH. Using the probe it is possible to visualize the CE-mediated acidification of hepatoma cells and hepatic tissues during medication with antipyretic anti-inflammatory drugs.

Carboxylesterase (CE) is an important enzyme for ester drugs including antipyretic and anti-inflammatory medicines.[1] CE mainly exists in the endoplasmic reticulum as well as mitochondria. These two organelles are in close contact, resulting in high levels of CE near the mitochondria.[2] During the metabolism of these drugs, CE participates in the hydrolysis of esters and the resultant acidic metabolites may cause the acidification of mitochondria. Mitochondria are one of the most vital organelles in cells,[3] and their acidification is extremely dangerous especially for mitochondrial division.[4] Therefore, exploring CE-mediated mitochondrial acidification is essential for understanding the enzyme triggered organelle aberrations.

During drug administration, the acidification of mitochondria can be caused by CE-generated metabolites. Therefore, a molecular probe is required that can successively respond to CE activity and pH, in order to visually explore CE-mediated pH variation during the administration of ester drugs. For many years, researchers have developed various molecular probes,[5] many of which can be used for report CE activity[6] or pH.[7] Unfortunately, there is no molecular probe for the consecutive reporting of CE activity and pH. Therefore, with this research, we present the design of a ratiometric two-photon fluorescent probe for the *in situ* imaging the CE activity and pH in mitochondria.

Mitochondria-targeting groups are usually positive groups, that can exit the mitochondria during cellular acidification, therefore causing a loss of *in situ* information about the mitochondria. Therefore, with our design, we synthesized the 1-(4-(chloromethyl)benzyl)-4-methylpyridin-1-ium with 4-methylpyridine and 1,4-bis(chloromethyl)benzene (Fig. S1, ESI†). This molecule has both a positive charge for mitochondria targeting and a benzyl chloride group that can covalently lock the probe with the mitochondria, allowing for the *in situ* evaluation of mitochondrial information even under the acidic conditions. With this precursor, we next obtained the (E)-1-(4-(chloromethyl)benzyl)-4-(2-(7-hydroxy-2-oxo-2H-chromen-3-yl)pyridin-1-ium (**HMT**)). **HMT** responds to changes of pH in a reversible ratiometric manner. Finally, we transformed the hydroxyl of **HMT** into carboxylic esters to produce the **CEMT** probe. According to our design, **CEMT** can target and lock with the mitochondria, and be triggered by mitochondrial CE to produce **HMT** which can then reversibly monitor the variation of pH in the mitochondria (Scheme 1).

With the probe **CEMT** in hand, we investigated its properties. Fig. 1 shows that, with the increase of CE, the emission of **CEMT** at 460 nm (Ex = 410 nm) decreases gradually while the emission

*[a] The Key Laboratory of Life-Organic Analysis, Key Laboratory of Pharmaceutical Intermediates and Analysis of Natural Medicine, College of Chemistry and Chemical Engineering, Qufu Normal University, The school attached to Qufu Normal University, Qufu 273165, China. E-mail: chenandguang@163.com*

*[b] Key Laboratory of Tibetan Medicine Research & Qinghai Key Laboratory of Qinghai-Tibet Plateau Biological Resources, Northwest Institute of Plateau Biology, Chinese Academy of Science, Xining 810001, Qinghai, P. R. China*

*[c] Department of Chemistry, University of Bath, Bath, BA2 7AY, UK. E-mail: t.d.james@bath.ac.uk*

† Electronic supplementary information (ESI) available. See DOI: 10.1039/c9cc05759e

**Scheme 1** Design and sensing mechanism of a ratiometric two-photon mitochondria-locked probe **CEMT** toward carboxylesterase (CE) activity and pH.
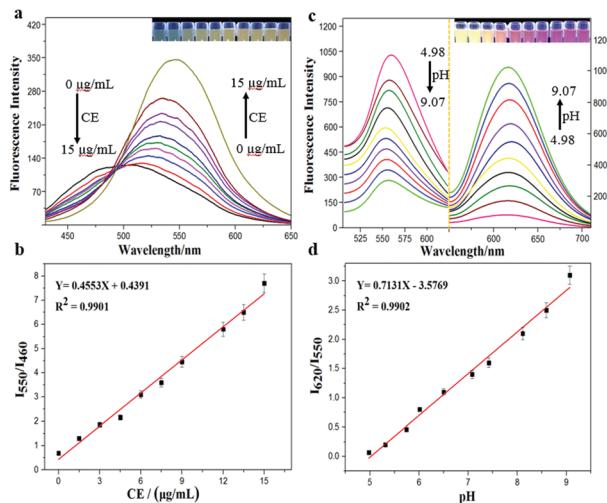
Fig. 1 Optical response to CE activity and pH. (a) Fluorescence spectra changes and (b) fluorescent intensity ratio ($I_{550}/I_{460}$) of **CEMT** (10 µM) in the presence of carboxylesterase (0 µg mL$^{-1}$, 1.5 µg mL$^{-1}$, 3.0 µg mL$^{-1}$, 4.5 µg mL$^{-1}$, 6.0 µg mL$^{-1}$, 7.5 µg mL$^{-1}$, 9.0 µg mL$^{-1}$, 12.0 µg mL$^{-1}$, 13.5 µg mL$^{-1}$, 15.0 µg mL$^{-1}$) in B–R buffer solution (pH = 7.42, 40 mM) at 37 °C. $\lambda_{ex}$ = 410 nm. (c) Fluorescence spectra changes and (d) fluorescent intensity ratio ($I_{620}/I_{550}$) of HMT (10 µM) in the presence of in 40 mM B–R buffer solution at various pH (4.98, 5.31, 5.74, 6.01, 6.50, 7.08, 7.42, 8.31, 8.59, 9.07) ($\lambda_{ex}$ = 410 nm and 530 nm).

at 550 nm (Ex = 410 nm) increases linearly ($I_{550}/I_{460}$). The ratiometric response of ultraviolet absorption is observed (Fig. S4, ESI†), which is consistent with the fluorescence properties. Next, we investigated the fluorescence response of **HMT** to pH.

As Fig. 1 indicates, with increasing pH (5.0–9.0), the fluorescence intensity of **HMT** at 550 nm decreases, while the fluorescence intensity at 620 nm (Ex = 530 nm) increases, with good linear correlation towards pH for the $I_{620}/I_{550}$ ratio. The reversibility for reporting pH was satisfactory (Fig. S7, ESI†). We then evaluated the ability of **CEMT** to report CE activity and pH. As shown in Fig. 2, **CEMT** displayed a ratiometric response ($I_{550}/I_{460}$) towards increasing amounts of CE (0–15 µg mL$^{-1}$). Subsequently, B–R buffer was added to generate pH values from 5.0 to 9.0, resulting in a ratiometric response ($I_{620}/I_{550}$). Thus, **CEMT** was suitable for the consecutive reporting of CE activity and pH. Finally, we validated the ability of **CEMT** to target and lock at the mitochondria. As shown in Fig. 3, the co-localization
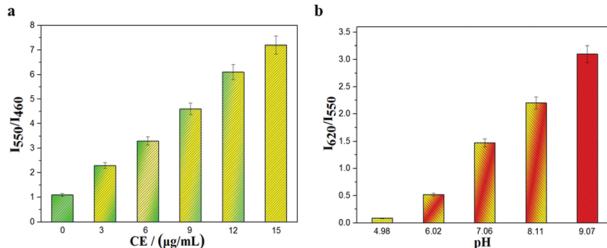


Fig. 2 (a) Fluorescence ratio of probe **CEMT** (10.0 µM) in B–R buffer solution (pH = 7.42, 40 mM) toward CE (0, 3.1, 6.0, 9.2, 11.9 and 15.0 µg mL$^{-1}$). (b) B–R buffer was added to the resulting mixture of (a) to give a pH values of 4.98–9.07 ($\lambda_{ex}$ = 410 nm and 530 nm).
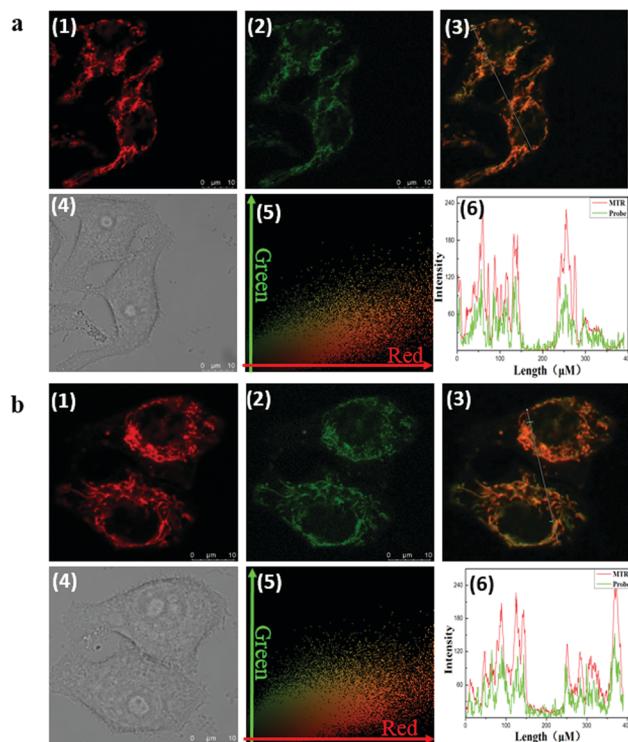


Fig. 3 Colocalization experiments of probe HMT and Mito Tracker Deep Red (MTDR) in HepG2 cells. The cells were incubated with HMT (10 µM) for 20 min at 37 °C ((a): pH = 7.40; (b): pH = 4.98), and the medium was replaced with fresh medium containing MTDR (0.1 µM) and incubated for 15 min. Images for MTDR (1) and HMT (2) were then recorded using excitation wavelengths of 633 and 488 nm, and collection windows were at 660–740 nm and 500–570 nm, respectively. (3) The merged images of (1) and (2). (4) The bright field. (5) The correlation between red and green channels in (3). (6) Pixel correlation across arrow in (3). Scale bar: 10 µm.

experiments of **HMT** with MTDR (mitochondrial targeting deep red dye: Ex = 640 nm; Em = 662 nm) indicates that the Pearson's co-localization coefficient was 0.91, demonstrating good targeting ability of **CEMT**. Subsequently, we changed the pH to 5.0 with B–R buffer and obtained the co-localization coefficients of **HMT** with MTDR as 0.89. These results demonstrate that although the mitochondria were acidified, probe leakage from the mitochondria was negligible. Therefore, **CEMT** can be used for the *in situ* imaging of mitochondrial CE activity and pH.

Therefore, we investigated the ability of **CEMT** to image CE-mediated acidification in cells. As shown in Fig. 4-1, the control group exhibited fluorescence in the yellow channel and the red channel. The two ratios, R1 ($I_{550}/I_{460}$) and R2 ($I_{620}/I_{550}$), indicate the CE activity and pH (Fig. 4-1). Then, enzyme inhibitor BNPP (bis-para-nitrophenylphosphate) was added to group 2 before incubation with **CEMT**. As shown in Fig. 4-2, compared to the control group, fluorescence of the green channel was significantly enhanced, while the fluorescence of both yellow channel and red channel was very weak. This result indicated that BNPP effectively inhibited CE activity, which confirmed that the yellow fluorescence in the control group was due to CE activity. In group 3, we added vinyl acetate, a well-known CE-mediated acidizing agent,[8] to investigate the response pattern of **CEMT** to
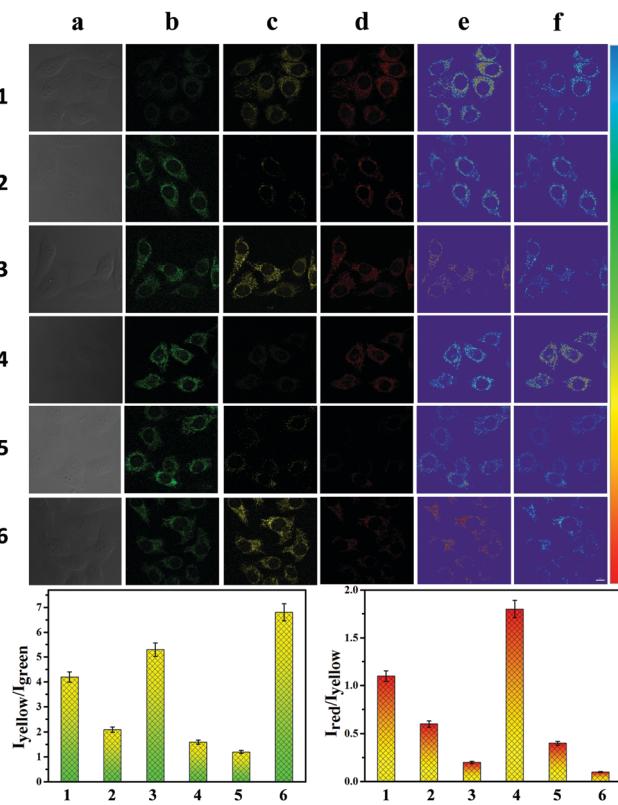
**Fig. 4** Two-photon fluorescence images of HepG2 cells. (1) HepG2 cells incubated with **CEMT** (10 μM) for 20 min. (2) HepG2 cells pre-treated with BNPP (500 μM) before incubation with **CEMT** (10 μM) for 20 min. (3) HepG2 cells pre-treated with vinyl acetate (500 μM) before incubation with **CEMT** (10 μM) for 20 min. (4). HepG2 cells pre-treated with BNPP (500 μM) before the incubation with vinyl acetate (500 μM) for 20 min, followed by incubation with **CEMT** (10 μM) for 20 min. (5). HepG2 cells pre-treated with BNPP (500 μM) before incubation with B–R buffer (pH = 4.98, 40 mM) for 20 min, followed by incubation with **CEMT** (10 μM) for 20 min. (6). HepG2 cells pre-treated with benorilate (500 μM) for 20 min before incubation with **CEMT** (10 μM) for 20 min. Images were captured using 810 nm for two-photon excitation. Two-photon fluorescence emission window: (a) bright field. (b) Green channel (400–500 nm). (c) Yellow channel (500–570 nm). (d) Red channel (570–710 nm). (e) Ratio imaging: $I_{yellow}/I_{green}$. (f) Ratio imaging: $I_{red}/I_{yellow}$. Scale bar: 20 μm.

**CE activity and pH.** Compared with group 1, group 3 exhibited an enhanced green fluorescence intensity, indicating that CE participated in the metabolism of vinyl acetate and the activity of the CE decreased. However, the yellow fluorescence increased with decreasing red fluorescence, indicating that the metabolism of vinyl acetate resulted in a lowering of the pH. Accordingly, the two ratios R1 ($I_{550}/I_{460}$) and R2 ($I_{620}/I_{550}$), displayed upward and downward trends respectively (Fig. 4-3). To verify the result, we pre-treated the cells with inhibitor BNNP before incubation with vinyl acetate. From Fig. 4-4, we can see that, compared with group 3, this group displayed an enhanced fluorescence in the green channel and a weakened fluorescence in yellow channel, demonstrating the inhibition of CE. Finally, to verify that acidification was caused by the CE mediated metabolism of vinyl acetate, we used the B-R buffer to adjust the pH to 5.0 after the cells were pre-treated with BNNP. As

shown in Fig. 4-5, compared with group 3, this group displayed a strong fluorescence in green channel, weak fluorescence in the yellow channel and negligible fluorescence in the red channel. Indicating, that CE facilitates acidification *via* mediation of the metabolism of vinyl acetate. Thus, we can use the signal of **CEMT** to detect acidification caused by CE-mediated hydrolysis of ester drugs. As an antipyretic drug, benorilate is widely used in the clinic. CE can metabolize benorilate to the acetylsalicylic acid resulting in a reduction of fever and inflammation. We then used the benorilate instead of vinyl acetate to perform the above imaging analysis. As Fig. 4-6 shows, compared with the control group 1, group 6 exhibited enhanced fluorescence in both the green and the yellow channel but weakened fluorescence in the red channel. Obviously, benorilate results in similar fluorescence changes to vinyl acetate, which indicates that benorilate participates in the CE-mediated metabolism and causes acidification. Moreover, the increased R1 ($I_{550}/I_{460}$) and the decreased R2 ($I_{620}/I_{550}$) further confirmed this result. Therefore, with its dual ratio signals, **CEMT** is able to reveal CE-mediated mitochondrial acidification. Considering the two-photon nature of **CEMT**, we then set out to test its applicability for tissue imaging. Since, the liver is responsible for drug metabolism, we used the probe to visualize the CE-mediated acidification during medication. Drug medication was performed with mice *via* the heart perfusion of vinyl acetate or benorilate (ESI†). As shown in Fig. 5, compared with group 1, group 2 (vinyl acetate) and group 3 (benorilate) displayed increased fluorescence intensity in the green channel, indicating a decreased activity of CE due to its participation in drug metabolism.
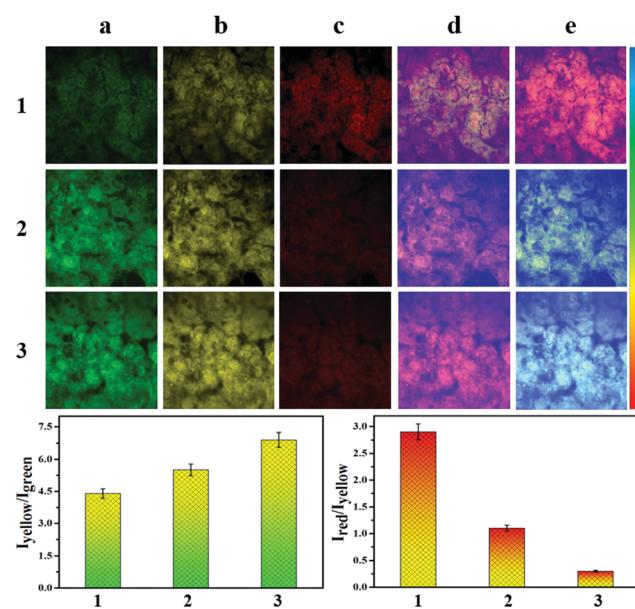


**Fig. 5** Two-photon fluorescence images for liver of mice with cardiac perfusion: (1) **CEMT** (20 μM) for 10 min. (2) Pretreated with vinyl acetate (1 mM) before with **CEMT** (20 μM). (3) Pretreated with benorilate (1 mM) before with **CEMT** (20 μM) for 10 min. Images were captured using 810 nm for two-photon excitation. Emission window: (a) green channel (400–500 nm). (b) Yellow channel (500–570 nm). (c) Red channel (570–710 nm). (d) Ratio imaging: $I_{yellow}/I_{green}$. (e) Ratio imaging: $I_{red}/I_{yellow}$. Scale bar: 20 μm.

Moreover, the fluorescence ratios $I_{yellow}/I_{green}$ and $I_{red}/I_{yellow}$ exhibited upwards and downwards trends respectively. Thus, the two sets of data consistently demonstrated the CE mediated acidification during medication with ester drugs.

In summary, a dual ratiometric mitochondria-locked two-photon fluorescent molecular probe **CEMT** has been designed to detect CE activity and pH. During medication with ester drugs, **CEMT** responded to CE-mediated acidification with an upward R1 ($I_{550}/I_{460}$) and downward R2 ($I_{620}/I_{550}$). Moreover, the mitochondrial targeting function allowed visualization of *in situ* information during acidification. The **CEMT** probe is an effective tool for the visualization of the CE-mediated acidification of cells and tissue, which is of great significance for the exploration of subcellular environmental changes mediated by enzymes.

## Conflicts of interest

There are no conflicts to declare.

## Notes and references

1 M. Gutova, G. M. Shackleford, V. Khankaldyyan, K. A. Herrmann, X. H. Shi, K. Mittelholtz, Y. Abramyants, M. S. Blanchard, S. U. Kim, A. J. Annala, J. Najbauer, T. W. Synold, M. D'Apuzzo, M. E. Barish, R. A. Moats and K. S. Aboody, *Gene Ther.*, 2012, **20**, 143.
2 (a) M. Hamasaki, N. Furuta, A. Matsuda, A. Nezu, A. Yamamoto, N. Fujita, H. Oomori, T. Noda, T. Haraguchi, Y. Hiraoka, A. Amano and T. Yoshimori, *Nature*, 2013, **495**, 389; (b) R. Malli and W. F. Graier, *Nat. Cell Biol.*, 2019, **21**, 667–668.
3 T. Lieber, S. P. Jeedigunta, J. M. Palozzi, R. Lehmann and T. R. Hurd, *Nature*, 2019, **570**, 380–384.
4 J. E. Lee, L. M. Westrate, H. Wu, C. Page and G. K. Voeltz, *Nature*, 2016, **540**, 139.
5 (a) S. Erbas-Cakmak, S. Kolemen, A. C. Sedgwick, T. Gunnlaugsson, T. D. James, J. Yoon and E. U. Akkaya, *Chem. Soc. Rev.*, 2018, **47**, 2228–2248; (b) H.-W. Liu, L. Chen, C. Xu, Z. Li, H. Zhang, X.-B. Zhang and W. Tan, *Chem. Soc. Rev.*, 2018, **47**, 7140–7180; (c) J. Ning, W. Wang, G. Ge, P. Chu, F. Long, Y. Yang, Y. Peng, L. Feng, X. Ma and T. D. James, *Angew. Chem., Int. Ed.*, 2019, **58**, 9959; (d) W. Zhang, J. Zhang, P. Li, J. Liu, D. Su and B. Tang, *Chem. Sci.*, 2019, **10**, 879–883; (e) X. Wang, P. Li, Q. Ding, C. Wu, W. Zhang and B. Tang, *J. Am. Chem. Soc.*, 2019, **141**, 2061–2068; (f) J. Ning, T. Liu, P. Dong, W. Wang, G. Ge, B. Wang, Z. Yu, L. Shi, X. Tian, X. Huo, L. Feng, C. Wang, C. Sun, J. Cui, T. D. James and X. Ma, *J. Am. Chem. Soc.*, 2019, **141**, 1126–1134; (g) F. Ding, Z. Chen, W. Y. Kim, A. Sharma, C. Li, Q. Ouyang, H. Zhu, G. Yang, Y. Sun and J. S. Kim, *Chem. Sci.*, 2019, **10**, 7023–7028; (h) Z. Liu, X. Zhou, Y. Miao, Y. Hu, N. Kwon, X. Wu and J. Yoon, *Angew. Chem., Int. Ed.*, 2017, **56**, 5812–5816; (i) K. Dou, Q. Fu, G. Chen, F. Yu, Y. Liu, Z. Cao, G. Li, X. Zhao, L. Xia, L. Chen, H. Wang and J. You, *Biomaterials*, 2017, **133**, 82–93.
6 (a) E. A. Halabi, Z. Thiel, N. Trapp, D. Pinotsi and P. Rivera-Fuentes, *J. Am. Chem. Soc.*, 2017, **139**, 13200–13207; (b) S. J. Park, H. W. Lee, H.-R. Kim, C. Kang and H. M. Kim, *Chem. Sci.*, 2016, **7**, 3703–3709; (c) Q. Jin, L. Feng, D.-D. Wang, Z.-R. Dai, P. Wang, L.-W. Zou, Z.-H. Liu, J.-Y. Wang, Y. Yu, G.-B. Ge, J.-N. Cui and L. Yang, *ACS Appl. Mater. Interfaces*, 2015, **7**, 28474–28481; (d) Q. Jin, L. Feng, D.-D. Wang, J.-J. Wu, J. Hou, Z.-R. Dai, S.-G. Sun, J.-Y. Wang, G.-B. Ge, J.-N. Cui and L. Yang, *Biosens. Bioelectron.*, 2016, **83**, 193–199; (e) L. Feng, Z.-M. Liu, L. Xu, X. Lv, J. Ning, J. Hou, G.-B. Ge, J.-N. Cui and L. Yang, *Chem. Commun.*, 2014, **50**, 14519–14522; (f) W. Chyan and R. T. Raines, *ACS Chem. Biol.*, 2018, **13**, 1810–1823; (g) S. J. Park, Y. J. Kim, J. S. Kang, I. Y. Kim, K. S. Choi and H. M. Kim, *Anal. Chem.*, 2018, **90**, 9465–9471; (h) D.-D. Wang, Q. Jin, L.-W. Zou, J. Hou, X. Lv, W. Lei, H.-L. Cheng, G.-B. Ge and L. Yang, *Chem. Commun.*, 2016, **52**, 3183–3186; (i) J. Wang, Q. Chen, N. Tian, W. Zhu, H. Zou, X. Wang, X. Li, X. Fan, G. Jiang and B. Z. Tang, *J. Mater. Chem. B*, 2018, **6**, 1595–1599.
7 (a) A. Wallabregue, D. Moreau, P. Sherin, P. Moneva Lorente, Z. Jarolímová, E. Bakker, E. Vauthey, J. Gruenberg and J. Lacour, *J. Am. Chem. Soc.*, 2016, **138**, 1752–1755; (b) D. Xu, Y. Li, C.-Y. Poon, H.-N. Chan, H.-W. Li and M. S. Wong, *Anal. Chem.*, 2018, **90**, 8800–8806; (c) M. H. Lee, N. Park, C. Yi, J. H. Han, J. H. Hong, K. P. Kim, D. H. Kang, J. L. Sessler, C. Kang and J. S. Kim, *J. Am. Chem. Soc.*, 2014, **136**, 14136–14142; (d) A. R. Sarkar, C. H. Heo, L. Xu, H. W. Lee, H. Y. Si, J. W. Byun and H. M. Kim, *Chem. Sci.*, 2016, **7**, 766–773; (e) X. Liu, Y. Su, H. Tian, L. Yang, H. Zhang, X. Song and J. W. Foley, *Anal. Chem.*, 2017, **89**, 7038–7045; (f) M.-Y. Wu, K. Li, Y.-H. Liu, K.-K. Yu, Y.-M. Xie, X.-D. Zhou and X.-Q. Yu, *Biomaterials*, 2015, **53**, 669–678; (g) L. Wang, X. Zhu, C. Xie, N. Ding, X. Weng, W. Lu, X. Wei and C. Li, *Chem. Commun.*, 2012, **48**, 11677–11679; (h) G. Chen, Q. Fu, F. Yu, R. Ren, Y. Liu, Z. Cao, G. Li, X. Zhao, L. Chen, H. Wang and J. You, *Anal. Chem.*, 2017, **89**, 8509–8516; (i) A.-M. Luo, Y. Shao, K.-J. Zhang, Y.-W. Wang and Y. Peng, *Chin. Chem. Lett.*, 2017, **28**, 2009–2013; (j) X. Sun, Y.-W. Wang and Y. Peng, *Org. Lett.*, 2012, **14**, 3420–3423.
8 J. R. Kuykendall, M. L. Taylor and M. S. Bogdanffy, *Toxicol. Appl. Pharmacol.*, 1993, **123**, 283–292.